Fuel 109 (2013) 575–581

Contents lists available at SciVerse ScienceDirect

Fuel

journal homepage: www.elsevier.com/locate/fuel

Nitrogen removal from natural gas using solid boron: A first-principles computational study

Qiao Sun [a,*], Meng Wang [b], Zhen Li [c,*], Ping Li [d], Weihua Wang [d], Xiaojun Tan [e], Aijun Du [f,*]

[a] Centre for Theoretical Computational Molecular Science, Australian Institute for Bioengineering and Nanotechnology, The University of Queensland, QLD 4072, Brisbane, Australia
[b] Center for Bioengineering and Biotechnology, China University of Petroleum (East China), Qingdao 266555, China
[c] Institute of Superconducting & Electronic Materials, The University of Wollongong, NSW 2500, Australia
[d] School of Chemistry and Chemical Engineering, Qufu Normal University, Qufu, Shandong 273165, China
[e] College of Medical and Life Science, University of Jinan, Jinan, Shandong 250022, China
[f] School of Chemistry, Physics and Mechanical Engineering, Queensland University of Technology, Brisbane, QLD 4001, Australia

HIGHLIGHTS

- CH_4 molecules can only form weak interactions with B_{12} cluster, α-B_{12} and γ-B_{28} surfaces.
- N_2 forms relative strong interaction with these boron adsorbents.
- These boron adsorbents have very high selectiveness to capture N_2 from natural gas.
- The boron adsorbents can be promising materials for natural gas purification.

GRAPHICAL ABSTRACT

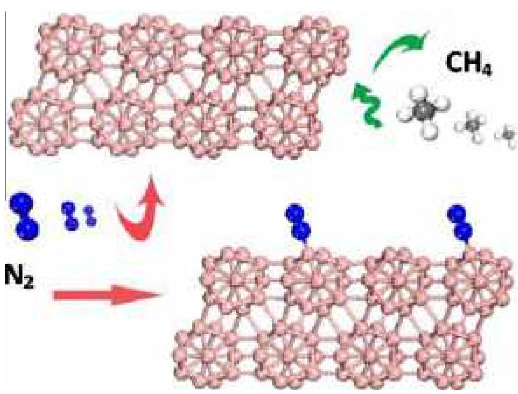

ARTICLE INFO

Article history:
Received 3 December 2012
Received in revised form 14 March 2013
Accepted 15 March 2013
Available online 1 April 2013

Keywords:
N_2/CH_4 separation
Gas purification
DFT calculations

ABSTRACT

Selective separation of nitrogen (N_2) from methane (CH_4) is highly significant in natural gas purification, and it is very challenging to achieve this because of their nearly identical size (the molecular diameters of N_2 and CH_4 are 3.64 Å and 3.80 Å, respectively). Here we theoretically study the adsorption of N_2 and CH_4 on B_{12} cluster and solid boron surfaces α-B_{12} and γ-B_{28}. Our results show that these electron-deficiency boron materials have higher selectivity in adsorbing and capturing N_2 than CH_4, which provides very useful information for experimentally exploiting boron materials for natural gas purification.

1. Introduction

The demand for natural gas is expected to increase continuously in the coming years, because natural gas produces lower CO_2 emission than other fossil fuels. Novel transport technologies, the remarkable reserves found, the lower overall costs and the environmental sustainability all point to natural gas as the primary energy source in the near future [1,2]. In fact, the demand for natural gas may exceed coal by 2020, due to its less pollution and higher use efficiency [3]. The natural gas reservoirs are usually far from final markets, and as a consequence it has to be transported either by pipelines as a gaseous mixture containing at least 75% of methane, or by tankers as liquified natural gas containing at least 85% of methane [4]. The choice between the two transportation

* Corresponding authors. Tel.: +61 7 33463996; fax: +61 7 33463992 (Q. Sun).
E-mail addresses: q.sun@uq.edu.au (Q. Sun), zhenl@uow.edu.au (Z. Li), aijun.du@qut.edu.au (A. Du).

0016-2361/$ - see front matter © 2013 Elsevier Ltd. All rights reserved.
http://dx.doi.org/10.1016/j.fuel.2013.03.032

technologies depends mainly on the distance and the volume of gas to be transferred.

Nitrogen is a common contaminant in natural gas and is quite difficult to be removed. It lowers the value of the natural gas and makes it untransportable to most pipelines. Natural gas can be accepted for pipeline transport-only it contains less amount of nitrogen, typically between 4% and 6%. Therefore several approaches (e.g. cryogenic separation, solid adsorption and membrane separation) have been developed for removing nitrogen. Cryogenic nitrogen removal is complex and expensive, prohibiting large-scale purification of natural gas [5]. Solid adsorption has been proposed as attractive alternatives for natural gas purification. However, most sorbents show weak interactions with methane and nitrogen, and unable to effectively separate them [3]. Conventional membrane technology cannot effectively separate nitrogen from natural gas because of the similar molecules kinetic diameters of methane and nitrogen (σ_{N_2} = 3.64 Å, σ_{CH_4} = 3.80 Å) [6]. Thus, very few materials are able to selectively adsorb nitrogen from natural gas, and it is highly significant to seek new materials with high selectivity and low cost for separation of nitrogen from natural gas.

In recent years, novel boron clusters and boron crystals have attracted extensive attentions [7–15], due to their unique physicochemical properties [12,16–19]. There are growing interests in exploring the structures and properties of pure boron clusters and boron containing compounds because they have a wide variety of applications from nuclear reactors to superhard, thermoelectric and high energy materials. In the recent article "Boron Cluster Come of Age", Grimes commented the variety of boron clusters, such as neutral boranes, polyhedral boranes, and their derivatives, motivating us to reconsider the concept of covalent chemical bonding [20]. Among boron clusters, B_{12} icosahedron is the basic structural unit for the elementary boron solids (e.g. the well-known α-B_{12} and γ-B_{28} crystals) although the B_{12} icosahedron is not stable when it is treated as a single isolated cluster [21–24]. Recently, boron-rich ternary compounds containing B_{12} icosahedra have attracted considerable attention since they exhibit important features on both fundamental and practical perspectives [7,9,12,25–27].

For crystal boron, the central unit (i.e. B_{12} icosahedron) of their structures is same to that of many boron rich compounds, and can be flexibly linked, joined, or fused into rigid framework structures [12,16–18,21,25,26,28–31]. The formation of B_{12} unit and its versatile connectivity are attributed to the "electron deficiency", or hypovalency of boron. There are only four crystal phases reported for pure elementary boron: rhombohedral α-B_{12} [17,26,31] and β-B_{106} [16] (with 12 and 106 atoms in the unit cell, respectively), tetragonal T-192 [18] (with 190–192 atoms per unit cell) and γ-B_{28} (with 28 atoms in the unit cell). α-B_{12} consists of one B_{12} icosahedron per unit cell while γ-B_{28} consists of icosahedral B_{12} clusters and B_2 pairs in a NaCl-type arrangement [12]. Moreover, the electronic properties of the B_2 pairs and B_{12} clusters in γ-B_{28} are different, resulting in the charge transfer between B_{12} clusters and B_2 pairs [12]. In this paper, we investigate the adsorption of N_2 and CH_4 on boron B_{12} icosahedron cluster and boron solid surfaces of α-B_{12} and γ-B_{28}. The primary motivation is to identify solid boron crystals as new sorbents for natural gas purification.

2. Computational methods

The first-principles density-functional theory [32,33] with long range dispersion correction [34] (DFT-D) calculations were carried out using DMol3 module in Materials Studio [35,36]. The boron cluster and boron solid surfaces were fully optimized in the given symmetry using generalized gradient approximation treated by Perdew–Burke–Ernzerhof exchange–correlation potential. An all electron double numerical atomic orbital augmented by *d*-polarization functions (DNP) was used as basis set. The self-consistent field (SCF) procedure was used with a convergence threshold of 10^{-6} a.u. on energy and electron density. The direct inversion of the iterative subspace technique developed by Pulay was used with a subspace size 6 to speed up SCF convergence on these large clusters [37]. In order to achieve the SCF convergence when the gap between the highest occupied molecular orbital and the lowest unoccupied molecular orbital (HOMO–LUMO) is small, thermal smearing using finite-temperature Fermi function of 0.005 a.u. was used. Geometry optimizations were performed with a convergence threshold of 0.002 a.u./Å on the gradient, 0.005 Å on displacements, and 10^{-5} a.u. on the energy. The real-space global cutoff radius was set to be 4.10 Å. For the B_{12} cluster, the cluster was placed in a sufficiently large supercell (20 Å × 20 Å × 20 Å) to avoid interactions with its periodic images. The cell parameters for α-B_{12} and γ-B_{28} used for the calculations are all optimized. The optimized cell parameters of α-B_{12} and γ-B_{28} are in good agreement with experimental measurements. In details, the optimized cell parameters of α-B_{12} are with the values of $a = b = c$ = 5.052 Å, $\alpha = \beta = \gamma$ = 57.76°, which are very close to the values of experimental measurement of $a = b = c$ = 5.064 Å, $\alpha = \beta = \gamma$ = 58.10° [38]. For γ-B_{28}, the optimized cell parameters are a = 5.042 Å, b = 5.598 Å, c = 6.914 Å, $\alpha = \beta = \gamma$ = 90.0°, which are also consistent with the experimental values of a = 5.054 Å, b = 5.612 Å, c = 6.987 Å, $\alpha = \beta = \gamma$ = 90.0° [12]. The 4 × 4 α-boron (001) and 2 × 2 γ-boron (001) surfaces were chosen with 15 Å vacuum in order to avoid interactions with its periodic images, and the slab thicknesses of α-B_{12} and γ-B_{28} are 8.012 Å and 6.914 Å, respectively. The fully relaxed α-B_{12} (001) surface with cell vectors is shown in Fig. 1. Here we need to point out that the (001) surface of the current study is in a rhombohedral setting and the (001) surfaces of earlier studies [26,31,38] are in hexagonal settings. The Brillouin zone was sampled by 6 × 6 × 1 k-points using the Monkhorst–Pack scheme. The calculations of N_2 and CH_4 adsorption on α-B_{12} (001) and γ-B_{28} (001) surfaces are based on the fully optimized surfaces. We have considered all the possible adsorption sites for N_2 and CH_4 adsorption on α-B_{12} and γ-B_{28} surfaces. What we discussed in the manuscript is the most stable adsorption site. The transition state between chemisorption and physisorption of N_2 was investigated using the complete LST (linear synchronous transit)/QST (quadratic synchronous transit) method [39] implemented in Dmol3 code.

The adsorption energy of N_2 and CH_4 on B_{12} cluster, α-B_{12} and γ-B_{28} surfaces are calculated from the following equation:

$$E_{ads} = (E_B + E_{gas}) - E_{B\text{-}gas} \quad (1)$$

where $E_{B\text{-}gas}$ is the total energy of boron adsorbent with adsorbed gas, E_B is the energy of isolated boron adsorbent, and E_{gas} is the energy of isolated gas molecule, such as N_2 and CH_4. Electron

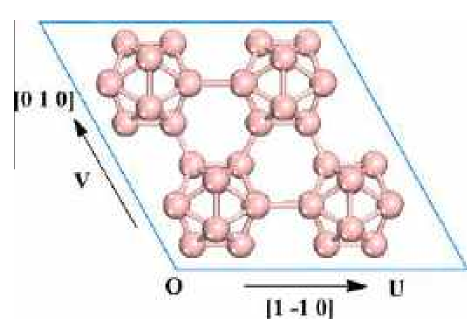

Fig. 1. The fully relaxed α-B_{12} (001) surface with cell vectors and the surface is in a rhombohedral setting. Atom color code: pink, boron. (For interpretation of the references to color in this figure legend, the reader is referred to the web version of this article.)

distribution and transfer mechanism are conducted by Mulliken method [40].

To better clarify the adsorption and the nature of the interaction of N_2 and CH_4 on B_{12} cluster, α-B_{12} and γ-B_{28} surfaces, the atoms in molecules (AIMs) theory which has been used to successfully determine intermolecular interactions of different systems has been employed using wavefunctions at B3LYP/6-311+G(d) level of theory [41–47]. The configurations for AIM calculations are based on the optimized structures at DFT-D level. In the AIM analyses, the existence of the interaction is indicated by the presence of a so-called bond critical point (BCP). The strength of the bond can be estimated from the magnitude of the electron density (ρ_{bcp}) at the BCP. Similarly, the ring or cage structures are characterized by the existence of a ring critical point (RCP) or cage critical point (CCP). Furthermore, the nature of the molecular interaction can be predicted from the topological parameters at the BCP, such as the Laplacian of electron density ($\nabla^2\rho_{bcp}$) and energy density (H_{bcp}). Generally, the sign of $\nabla^2\rho_{bcp}$ reveals whether charge is concentrated ($\nabla^2\rho_{bcp} < 0$) as in covalent bonds (shared interaction) or depleted ($\nabla^2\rho_{bcp} > 0$) as in ionic bonds, H-bonds, and van der Waals interactions (closed-shell interaction). The topological analysis of the system was carried out via the AIMALL program [48].

3. Results and discussions

Separation of N_2 from CH_4 is highly significant in natural gas purification. To the best of our knowledge, it is the first time to perform the first-principles DFT-D calculations of N_2 and CH_4 adsorption on B_{12} cluster, α-B_{12} and γ-B_{28}. Our results demonstrate the adsorption energies of N_2 on these materials are much higher than those of CH_4, which indicates the boron crystals have high selectivity in capturing N_2 from natural gas.

3.1. N_2 adsorption on B_{12} cluster, α-B_{12} and γ-B_{28}

In this part, we will discuss the DFT-D calculational results of N_2 adsorption on B_{12} icosahedron cluster, α-B_{12} and γ-B_{28} surfaces. We will start with the CH_4 adsorption on B_{12} cluster. The configurations of N_2 adsorption on B_{12} cluster are shown in Fig. 2. Correspondingly, the geometrical parameters and the physical and chemical adsorption energies are summarized in Table 1. For free N_2 molecule, the N–N bond length is calculated to be 1.109 Å. In its physisorbed configuration (Fig. 2a), N_2 is far from the B_{12} cluster with a distance of 2.990 Å. The molecular graphs of those geometries have been given in Fig. 3. As displayed in Fig. 3a, the interaction between N_2 and B_{12} cluster can be confirmed by the existence of the bond critical point (BCP) of the N_2–B contact. The corresponding topological parameters at the BCP have been presented in Table S2 in Supporting information. Obviously, the electron densities at the BCPs of the N_2–B between N_2 and B_{12} cluster are small (Table S2), which indicates the interaction is very weak and it is mainly come from the van der Waals interactions between N_2 and B_{12} cluster. Because of the weak interaction, the physisorbed N_2 molecule (N–N bond length = 1.110 Å) almost did not undergo noticeable structural change compared with the free N_2 (N–N bond length in gas phase is 1.109 Å). The Mulliken charge distributions of configurations of N_2 adsorption on B_{12} cluster and charge transfer between N_2 and B_{12} cluster are listed in Supporting information Table S1. The charge transfer from N_2 to B_{12} cluster is negligible and the value is -0.002e. The adsorption energy of N_2 molecule on B_{12} cluster is calculated to be 0.08 eV. In addition, our study also shows the physisorption process has no transition state.

In its chemisorption configuration (Fig. 2c), the distance between one boron atom in B_{12} cluster and one nitrogen atom in N_2 molecule is 1.515 Å. The adsorption energy is calculated to be 0.38 eV on PAW–PBE level, which suggests the chemisorption is a thermally favorable process. In the chemisorption, triple-bond of N_2 molecule is broken and slightly elongated to 1.132 Å on top of the B, compared with that of N_2 molecule in gas phase (with N–N bond length of 1.109 Å). The B–B bond connecting with N_2 is also considerably pulled out and elongated by 0.05 Å. Once the chemisorption is formed, there is 0.113 negative charge spontaneously transferring from N_2 molecules to B_{12} cluster because of "electron deficiency" of B_{12} cluster.

We performed LST/QST calculation to identify the transition state between physisorption and chemisorption configurations. As shown in Table S2, the electron densities at the BCPs for the N_2–B bonds of physisorption (Fig. 2a), transition state (Fig. 2b), and chemisorptions (Fig. 2c) increased gradually, which is consistently with the adsorption process from weak to strong interaction as well as the bond distances decrease from the values of 2.990 Å to 2.287 Å and 1.515 Å for the three structures, respectively. The imaginary frequency of the transition state is 130.4i cm^{-1} and it is assigned to the stretch mode of NN–B bond for formation of chemisorption configuration from its physisorption analogue. The results show the reactants need to overcome a barrier of 0.04 eV from the reaction path of its physisorption to chemisorption. The very low energy barrier for the reaction of N_2 adsorption from physisorption to chemisorption indicates that it is a kinetically favorable process.

In order to explore the application of boron crystals for natural gas separation, we also performed the DFT-D calculations of N_2 adsorption on α-B_{12} (001) and γ-B_{28} (001) surfaces. The configurations of N_2 adsorption on α-B_{12} and γ-B_{28} are shown in Fig. 2. Their important geometrical parameters and adsorption energies are also summarized in Table 1. In contrast to the *b* adsorption of N_2 on B_{12} cluster, we only gained chemisorption configurations for α-B_{12} and γ-B_{28} surfaces, in which N_2 molecules are tightly bound to the surface of α-B_{12} and γ-B_{28} with adsorption energies of 1.20 eV and 1.07 eV, respectively. In their configurations, the triple-bonds of N_2 molecules are broken and N–N bonds are slightly elongated to 1.126 Å and 1.124 Å on top of the B of α-B_{12} and γ-B_{28} surfaces, respectively. The B–B bonds connected with N_2 are also considerably elongated around 0.06–0.13 Å of the two surfaces. The distances between B atom and N atom are 1.469 Å and 1.479 Å for α-B_{12} and γ-B_{28}, respectively, which are shorter than that of N_2 adsorption on B_{12} cluster. This indicates the stronger interactions of N_2 with α-B_{12} and γ-B_{28}, which can be supported by the relatively larger electron densities at the BCPs for the N_2–B bond of the two configurations. Once the chemisorptions are formed, there are 0.141 negative charges spontaneously transferring from N_2 to α-B_{12} and γ-B_{28} because of "electron deficiency" of the boron solid. Our results demonstrate those chemisorption reactions have no transition state and the reactions are no barrier, and the adsorptions are kinetically favorable. Therefore, N_2 molecules adsorption on α-B_{12} and γ-B_{28} surfaces are energetically and kinetically favorable processes. The adsorption of N_2 on α-B_{12} surface is slightly more favorable than that of on γ-B_{28} surface. Here we need to mention that McElligott and Roberts' study showed that N_2 did not chemisorb on boron films of amorphous boron [49], while our calculational results indicate that N_2 molecules can form chemical bindings with α-B_{12} and γ-B_{28} crystal surfaces. The reason of the adsorption properties of amorphous boron is different from the crystalline forms might be that, in amorphous boron, the boron icosahedra are bonded randomly to each other without long-range order, and there will be more deformations and form more covalent bonds in amorphous boron than that of crystal boron, and the adsorption sites in crystal boron might have more dangling bonds than that of amorphous boron, so the adsorption sites with more dangling bonds in crystal boron could form strong interaction with nitrogen while the amorphous boron cannot.

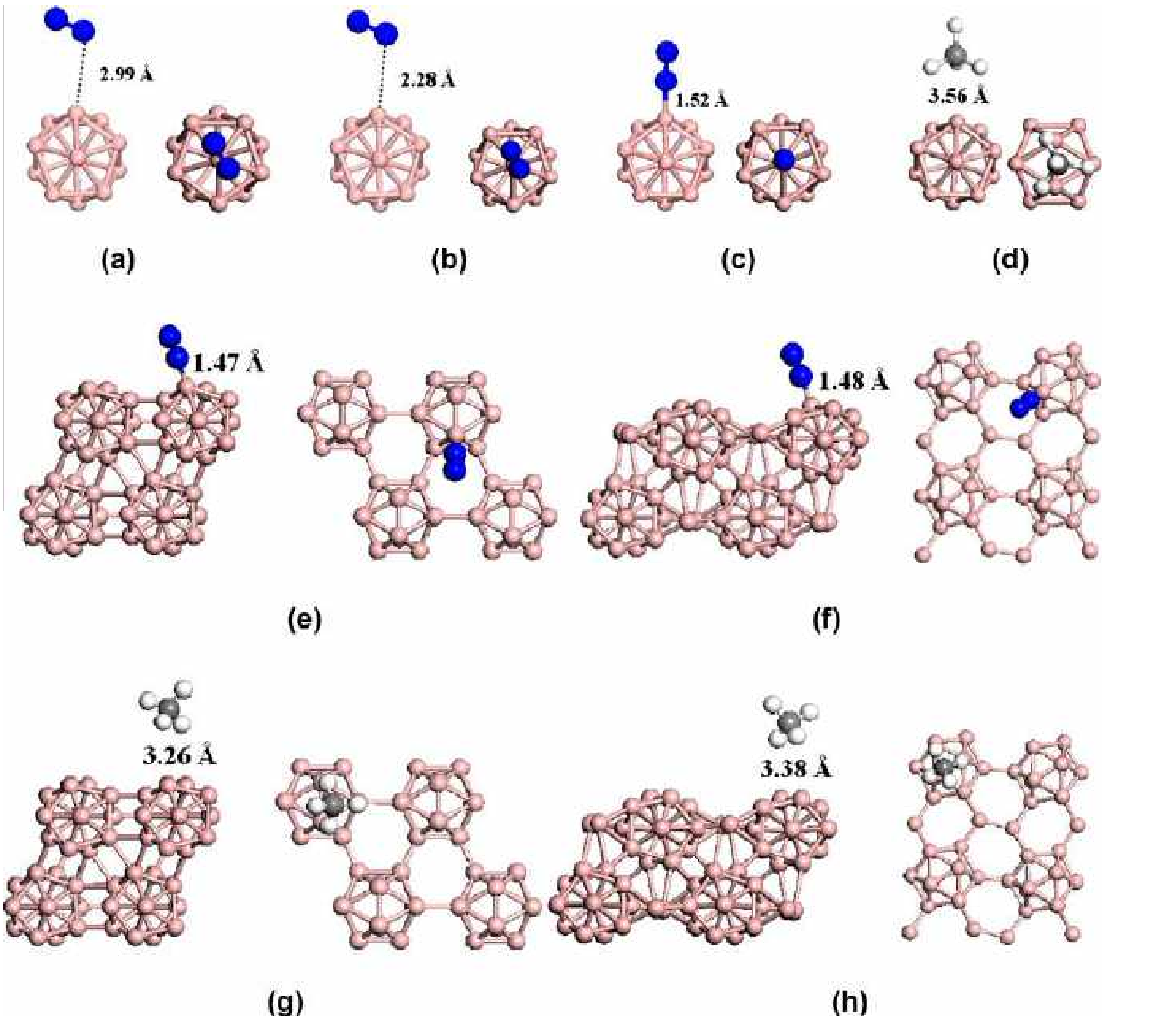

Fig. 2. (a–d) are side and top view of optimized configurations of N_2 and CH_4 adsorption on B_{12} cluster. (e–h) are side view of the slabs and top view of the surfaces of optimized configurations of N_2 and CH_4 adsorption on α-B_{12} and γ-B_{28}. Atom color code: blue, nitrogen; pink, boron; dark gray, carbon; light gray, hydrogen. (For interpretation of the references to color in this figure legend, the reader is referred to the web version of this article.)

Table 1
Adsorption energy in eV, bond distance (r) in Å and bond angle (α) in deg for N_2 adsorption on B_{12} cluster, α-B_{12} and γ-B_{28} surfaces.

Models		Physisorption	Transition state	Chemisorption
B_{12} cluster	Adsorption energy	0.08	0.04	0.38
	r(B···N)	2.990	2.287	1.515
	r(N–N)	1.110	1.117	1.132
	α (B–N–N)	115.0	132.3	178.6
α-B_{12}	Adsorption energy			1.20
	r(B···N)			1.469
	r(N–N)			1.126
	α (B–N–N)			175.2
γ-B_{28}	Adsorption energy			1.07
	r(B···N)			1.479
	r(N–N)			1.124
	α (B–N–N)			175.7

3.2. CH_4 adsorption on B_{12} cluster, α-B_{12} and γ-B_{28}

In order to understand the interaction properties between the boron materials and CH_4 molecules, we also calculated the adsorption of CH_4 on B_{12} cluster, α-B_{12} and γ-B_{28} surfaces. The calculated C–H bond length and H–C–H angle in free CH_4 molecule are 1.098 Å and 109.4°, respectively. In the following part, we will first discuss the adsorption of CH_4 on B_{12} cluster. The important structural parameters of CH_4 adsorption on B_{12} cluster are listed in Table 2. From the calculation we can only find CH_4 adsorbed on B_{12}

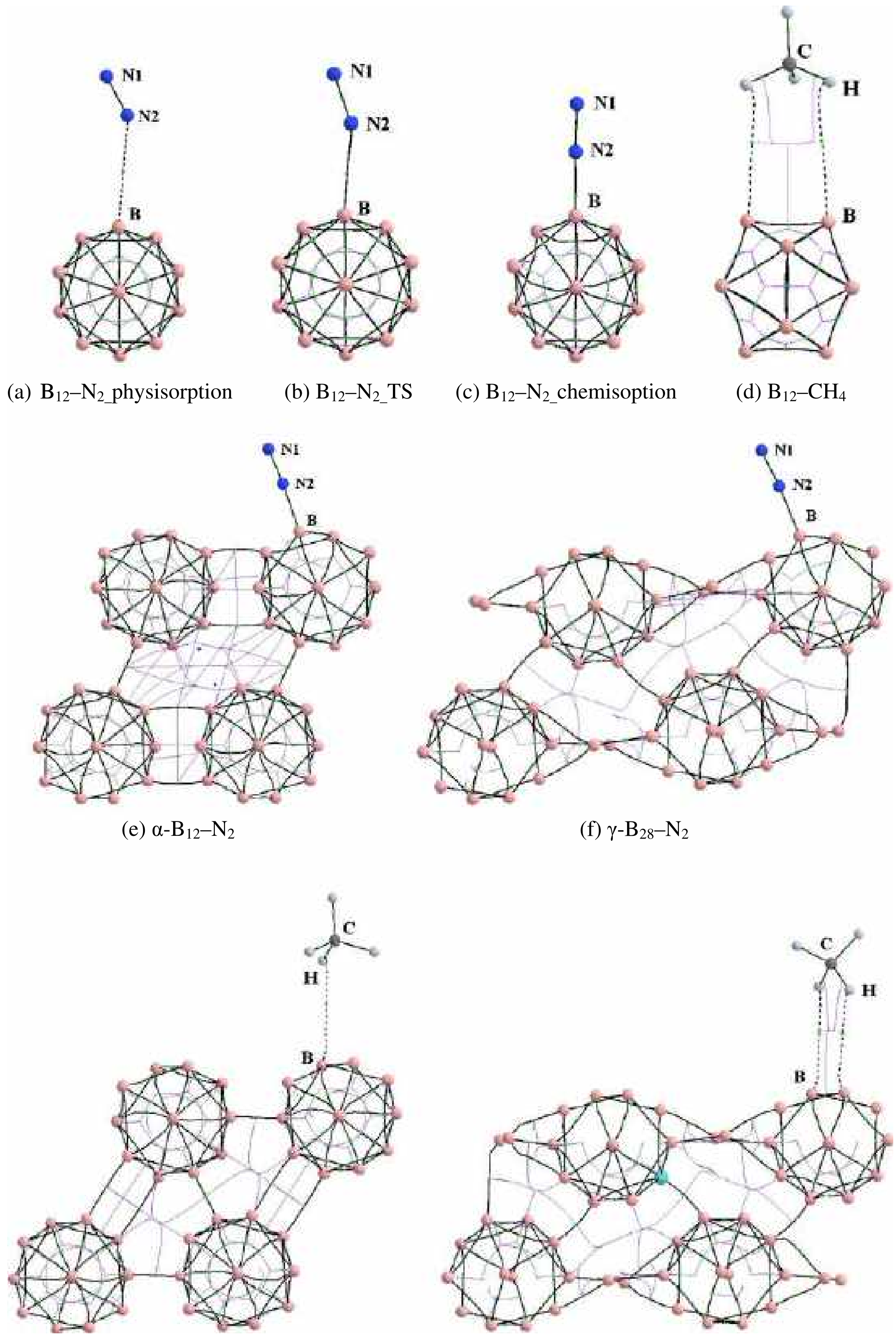

Fig. 3. The molecular graphs of the intermediates and transition state of N_2 and CH_4 adsorption on B_{12} cluster, α-B_{12} and γ-B_{28} surfaces, where the bond critical points (BCPs), ring critical points (RCPs) and cage critical point (CCP) are denoted as small green, red and blue dots, respectively. (For interpretation of the references to color in this figure legend, the reader is referred to the web version of this article.)

cluster by physisorbed configuration. The C···B and H···B distances of CH_4 on the sorbent are 3.557 Å and 2.833 Å, respectively. We can see that the distance between CH_4 and the adsorbent is quite far and the adsorption energy is only 0.08 eV. The charge transfer from CH_4 to B_{12} cluster is negligible and with the value of 0.002e (Table S1). These results indicate their interaction is very weak and it mainly arises from the van der Waals force between CH_4 and B_{12} cluster. Because of the weak interaction, the physisorbed CH_4 did

Table 2
Adsorption energy in eV, bond distance (r) in Å and bond angle (α) in deg for CH_4 adsorption on B_{12} cluster, α-B_{12} and γ-B_{28} surfaces.

	B_{12}	α-B_{12}	γ-B_{28}
Adsorption energy	0.08	0.17	0.14
r(B···C)	3.557	3.255	3.380
r(B···H)	2.833	2.807	2.676

not undergo noticeable structural changes compared with the geometry of free CH_4. The changes in two C–H bonds (1.098 Å) nearby B_{12} cluster are negligible compared with those of free CH_4 (1.099 Å). The same situation occurs for H–C–H angle which slightly decreases from 109.5° to 108.9°. As displayed in Fig. 3d, the interaction between CH_4 and B_{12} cluster can be confirmed by the existence of the bond critical point (BCP) of the H–B contact. Obviously, the electron densities at the BCPs of the H–B between CH_4 and B_{12} cluster are small (Table S2). Therefore CH_4 can be weakly adsorbed on B_{12} cluster, which is contrast to the adsorption of N_2 on B_{12} cluster.

The CH_4 adsorption on α-B_{12} and γ-B_{28} surfaces is also investigated for comparison. The important structural properties of CH_4 adsorption on α-B_{12} and γ-B_{28} are also listed in Table 2. From the calculational results we can see that the distances between CH_4 and α-B_{12}, γ-B_{28} sorbents are quite far. The C···B distances of CH_4 on α-B_{12} and γ-B_{28} are 3.255 Å and 3.380 Å, respectively, and H···B distances of CH_4 on α-B_{12} and γ-B_{28} are 2.807 Å and 2.676 Å, respectively. The charge transfer from CH_4 to α-B_{12} and γ-B_{28} are negligible and with the values of 0.006e and 0.014e, respectively. CH_4 is adsorbed on the two adsorbents by physical adsorption and the adsorption energies on α-B_{12} and γ-B_{28} are 0.17 eV and 0.14 eV, respectively. In addition, we can see from Table S2 that the electron densities at the BCPs of the H–B bonds between CH_4 and the two adsorbents are small, which are consistent with their weak interactions. In comparison with the interactions between N_2 and the two adsorbents, the interactions between CH_4 and α-B_{12} as well as γ-B_{28} are very weak. This demonstrates that α-B_{12} and γ-B_{28} have higher affinity to N_2 and they can be used to separate N_2 from N_2/CH_4 mixture.

The difference of adsorption energy among N_2 and CH_4 adsorbed on the three boron compounds can be understood by analysis of the energy-gaps between their highest occupied molecular orbitals (LUMOs) and lowest unoccupied molecular orbitals (HOMOs). According to the molecular orbital theory, the frontier orbits and nearby molecular orbits are the most important factors determining the stability of the molecule. The larger the difference between the LUMO–HOMO frontier orbits, the more stable the molecular structure is. The energy gaps of ΔE ($\Delta E = E_{\mathrm{LUMO}} - E_{\mathrm{HOMO}}$) for B_{12} cluster, α-B_{12} and γ-B_{28} surfaces are 2.103 eV, 0.046 eV and 0.854 eV, respectively. It is clearly observed the energy gaps of the three boron materials are in the order of α-B_{12} < γ-B_{28} < $B_{12\ \mathrm{cluster}}$. The narrower LUMO–HOMO energy-gap means the higher activity of molecule. The energy gaps of the three boron materials can explain the strength of the interactions of N_2 with the three sorbents which are in the order of α-B_{12} (adsorption energy 1.20 eV) > γ-B_{28} (adsorption energy 1.07 eV) > $B_{12\ \mathrm{cluster}}$ (adsorption energy 0.38 eV). Although the adsorption energies of CH_4 on B_{12} cluster, α-B_{12} and γ-B_{28} surfaces are in the same order, their values are very small (0.08–0.17 eV) and the interactions between CH_4 and all boron materials are very weak. The big differences of the adsorption energies of the two gases on the two boron crystals demonstrate that the boron crystals are very good materials for N_2/CH_4 separation. In addition, the selectivity of α-B_{12} is higher than that of γ-B_{28}. Moreover, from our results we can predict that other "electron deficiency" boron solids, such as β-B_{106} and T-192 could also be used as promising materials for natural gas purification.

4. Conclusions

In summary, we have calculated the adsorptions of CH_4 and N_2 on B_{12} cluster, α-B_{12} and γ-B_{28} surfaces. With all the three materials, CH_4 forms weak interactions with them and the adsorption energies are among 0.08–0.17 eV. However, N_2 molecules form strong chemical interactions with them and the adsorption energies of N_2 adsorption on B_{12} cluster, α-B_{12} and γ-B_{28} are 0.37, 1.20 and 1.07 eV, respectively. The results also show the adsorptions of N_2 on these boron sorbents have very low energy barrier or no energy barrier. The study demonstrates that "electron deficiency" boron crystals have high ability of N_2 capture and high selectivity for N_2/CH_4 mixture separation. These materials could serve as promising adsorbents for natural gas purification.

Acknowledgements

We are grateful to the Australian Research Council and China NSFC (21003082) for supporting this work. We also acknowledge generous grants of high performance computer time from both The University of Queensland and the National Computational Infrastructure (NCI).

Appendix A. Supplementary material

Supplementary data associated with this article can be found, in the online version, at http://dx.doi.org/10.1016/j.fuel.2013.03.032.

References

[1] Eni sustainability report; 2006. <http://www.eni.it>.
[2] Eni world oil & gas review; 2007. <http://www.eni.it>.
[3] Tagliabue M, Farrusseng D, Valencia S, Aguado S, Ravon U, Rizzo C, et al. Chem Eng J 2009;155:553.
[4] Kidnay AJ, Parrish WR. Fundamentals of natural gas processing. Boca Raton (USA): Taylor & Francis; 2006.
[5] Daimiger U, Lind W. Adsorption processes for natural gas treatment: a technology update. Engelhard Brochure; 2004.
[6] Breck DW. Zeolite molecular sieves. New York (USA): John Willey & Sons; 1974.
[7] Häussermann U, Mikhaylushkin AS. Inorg Chem 2010;49:11270.
[8] Zhao JJ, Wang L, Li FY, Chen ZF. J Phys Chem A 2010;114:9969.
[9] Oganov AR, Solozhenko VL. J Superhard Mater 2009;31:285.
[10] Li M, Li Y, Zhou Z, Shen P, Chen Z. Nano Lett 2009;9:1944.
[11] Zhao YF, Lusk MT, Dillon AC, Heben MJ, Zhang SB. Nano Lett 2008;8:157.
[12] Oganov AR, Chen J, Gatti C, Ma Y, Ma Y, Glass CW, et al. Nature 2009;457:863.
[13] Bean DE, Muya JT, Fowler PW, Minh Tho N, Ceulemans A. Phys Chem Chem Phys 2011;13:20855.
[14] Wang Y, Robinson GH. Science 2011;333:530.
[15] Gonzalez Szwacki N, Sadrzadeh A, Yakobson BI. Phys Rev Lett 2007;98:166804.
[16] Sands DE, Hoard JL. J Am Chem Soc 1957;79:5582.
[17] McCarty LV, Kasper JS, Horn FH, Decker BF, Newkirk AE. J Am Chem Soc 1958;80:2592.
[18] Talley CP. Acta Cryst 1960;13:271.
[19] Szwacki NG, Sadrzadeh A, Yakobson BI. Phys Rev Lett 2007;98:166804.
[20] Grimes RN. J Chem Educ 2004;81:658.
[21] Kawai R, Weare JH. J Chem Phys 1991;95:1151.
[22] Boustani I. Chem Phys Lett 1995;240:135.
[23] Boustani I. Phys Rev B 1997;55:16426.
[24] Zhai HJ, Kiran B, Li J, Wang LS. Nature Mater 2003;2:827.
[25] He JL, Wu ED, Wang HT, Liu RP, Tian YJ. Phys Rev Lett 2005;94:015504.
[26] Marlid B, Larsson K, Carlsson JO. J Phys Chem B 2001;105:12797.
[27] Wagner P, Ewels CP, Suarez-Martinez I, Guiot V, Cox SFJ, Lord JS, et al. Phys Rev B 2011;83:024101.
[28] Hubert H, Devouard B, Garvie LAJ, O'Keeffe M, Buseck PR, Petuskey WT, et al. Nature 1998;391:376.
[29] Franz R, Werheit H. Europhys Lett 1989;9:145.
[30] Li D, Xu YN, Ching WY. Phys Rev B 1992;45:5895.
[31] Decker BF, Kasper JS. Acta Cryst 1959;12:503.
[32] Zhao Y, Truhlar DG. J Chem Theory Comput 2007;3:289.
[33] Thanthiriwatte KS, Hohenstein EG, Burns LA, Sherrill CD. J Chem Theory Comput 2011;7:88.
[34] Grimme SJ. Comput Chem 2006;27:1787.
[35] Delley BJ. Chem Phys 1990;92:508.
[36] Delley BJ. Chem Phys 2000;113:7756.
[37] Pulay PJ. Comput Chem 1982;3:556.
[38] Will G, Kiefer B. Z Anorg Allg Chem 2001;627:2100.
[39] Halgren TA, Lipscomb WN. Chem Phys Lett 1977;49:225.
[40] Mulliken RS. J Chem Phys 1955;23:1833.
[41] Perdew JP, Wang Y. Phys Rev B 1992;45:13244.
[42] Altarawneh M, Dlugogorski BZ, Kennedy EM, Mackie JC. J Phys Chem A 2010;114:1098.

[43] Altarawneh M, Kennedy EM, Dlugogorski BZ, Mackie JC. J Phys Chem A 2008;112:6960.
[44] Sun Q, Bu YX, Qin M. J Phys Chem A 2003;107:1584.
[45] Sun Q, Doerr M, Li Z, Smith SC, Thiel W. Phys Chem Chem Phys 2010;12:2450.
[46] Sun Q, Li Z, Du A, Chen J, Zhu Z, Smith SC. Fuel 2012;96:291.
[47] Sun Q, Li Z, Wang M, Du A, Smith SC. Chem Phys Lett 2012;550:41.
[48] Bader RFW. Atoms in molecules: a quantum theory. New York: Oxford University Press; 1990.
[49] McElligo Pe, Roberts RW. J Chem Phys 1967;46:273.